Entanglement spectroscopy of anomalous surface states

Arjun Dey
Laboratory for Theoretical and Computational Physics, Paul Scherrer Institute, 5232 Villigen, Switzerland; Institute of Physics, École Polyetchnique Fédérale de Laussane (EPFL), 1015 Laussane, Switzerland; and Department of Condensed Matter Physics, Weizmann Institute of Science, Rehovot 7610001, Israel

David F. Mross
Department of Condensed Matter Physics, Weizmann Institute of Science, Rehovot 7610001, Israel

(Received 27 October 2022; revised 12 February 2024; accepted 13 February 2024; published 12 April 2024)

We study the entanglement spectra of surface states of symmetry-protected topological phases. The topological bulk imprints the surface with an anomaly that does not permit it to form a trivial "vacuum" state that is gapped, unfractionalized, and symmetry preserving. Any surface wave function encodes the topology of the underlying bulk in addition to a specific surface phase. We show that the real-space entanglement spectrum of such surface wave functions are dominated by the bulk topology and do not readily permit identifying the surface phase. We thus use a modified form of entanglement spectra that incorporates the anomaly and argue that they correspond to physical edge states between different surface states. We support these arguments by explicit analytical and numerical calculations for free and interacting surfaces of three-dimensional topological insulators of electrons.

DOI: 10.1103/PhysRevResearch.6.023047

I. INTRODUCTION

Over the past years, entanglement has surpassed the notion of correlations for characterizing and identifying quantum many-body systems. Famously, the entanglement entropy of two-dimensional gapped systems contains a universal contribution that is nontrivial for topologically ordered states [1,2]. This contribution vanishes for symmetry-protected topological states (SPTs), which do not host any fractional quasiparticles in the bulk. Still, their nontrivial topological nature can be deduced by resolving the entanglement entropy according to symmetries [3–5].

More refined information about topological states can be obtained from entanglement spectra (ES). In a seminal work, Li and Haldane [6] showed that the ES of certain quantum Hall states and their energy spectra at a physical edge are describable by the same conformal field theory. They argued that topological phases can thus be identified by their ES. Subsequently, such an ES-edge state correspondence has been proven for a broad class of two-dimensional topological states [7,8]. Additionally, the agreement of ES and physical edge spectra has been confirmed empirically for various other systems, including topological insulators [9,10], p-wave superfluids in the continuum [11] and on a lattice [12,13], fractional quantum Hall states [14–16], spin chains [17], and the Kitaev honeycomb model [18].

The conjectured ES-edge correspondence is a consequence of bulk-edge correspondence in gapped systems [7]. However, this bulk-edge correspondence does not directly apply to an essential and widely studied class of condensed-matter systems: Surface states of topological insulators or superconductors. Such states are characterized by bulk topological invariants that are different from the vacuum, i.e., they change discretely across the surface. Any SPT surface state must encode this change in topological invariants. When viewed as effective D-1 dimensional systems, the information about their topological origin yields an anomaly. They cannot be regularized in D-1 dimensions without breaking one of the symmetries protecting the SPT. Similarly, one cannot have a symmetric boundary between states with different anomalies (e.g., between a surface state and a trivial state).

These distinctive states, referred to as anomalous surface states in the literature [19,20], have been the subject of extensive investigation in the context of topological classification [21–24]. Some of the phases hosted by SPT surfaces have also been realized experimentally [25–27]. In fact, experimentally probing the surface states is typically the most efficient method for identifying the underlying bulk topology. Similarly, most theoretical analyses are based on effective surface theories. In particular, the interface between two gapped surface phases hosts topologically protected states, uniquely identifying one provided the other is known.

The basic problem with using entanglement spectra to identify surface states is illustrated in Fig. 1. When a conventional 2D system on a hollow sphere is physically cut along the equator, a 1D edge to vacuum is exposed, cf. Fig. 1(a). Depending on the 2D state, there may be topologically protected edge states. The same states can be obtained by a real-space

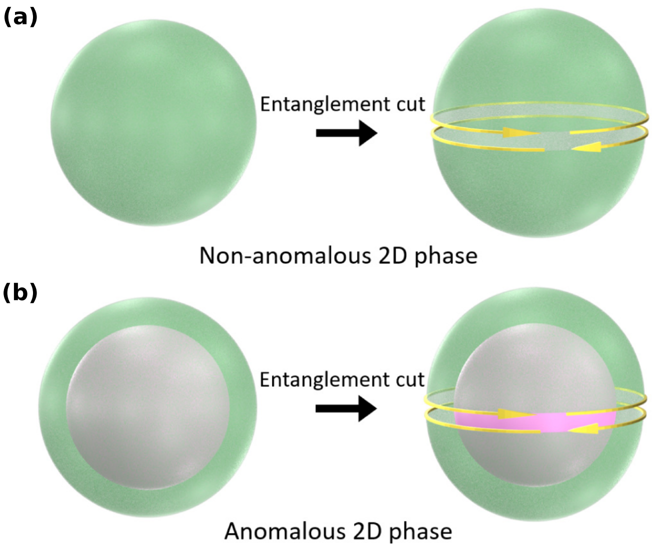

FIG. 1. (a) In a strictly two-dimensional system—represented here by a hollow spherical shell—a real-space entanglement cut mimics a physical cut: The entanglement spectrum matches the physical energy spectrum of one subsystem, which is dominated by one-dimensional edge channels [6–16]. (b) Surface states of a topological phase cannot be stripped off the bulk. An entanglement cut, on the surface only, mimics a physical cut on the surface layer but not on the bulk. Both expose the underlying topological bulk. Hence, the entanglement cut of a surface state does not isolate a one-dimensional edge.

entanglement cut between the two hemispheres. By contrast, an anomalous 2D surface state requires a 3D bulk, i.e., a solid sphere. In this case, it is not possible to separate the surface states into two hemispheres via a physical cut. Cutting the surface layer instead exposes part of the underlying bulk, revealing a new anomalous state that extends over the entire sphere. Similarly, we expect that the ES obtained after an entanglement cut of the anomalous surface wave function gets contaminated by the bulk, cf. Fig. 1(b). In this paper, we confirm this reasoning and show how entanglement spectroscopy can nevertheless identify the edge states between an arbitrary surface state and any known free-fermion state on the same surface.

As a concrete system for our numerical calculations, we use an electronic topological insulator (TI) with time-reversal symmetry $\mathcal{T}^2 = -1$ [28–30] as the paradigmatic example of a 3D SPT. When its two-dimensional surface is symmetric and noninteracting, it hosts a single two-component Dirac fermion [25,26]. This theory cannot arise in strictly two-dimensional systems with the same symmetries due to the parity anomaly [31,32] and can be seen as a consequence of fermion doubling [33–35]. When time-reversal symmetry is broken on the surface, the Dirac fermions become massive and realize a surface Hall conductance of $\sigma_{xy} = \frac{1}{2}$ [36,37] (in units of $\frac{e^2}{h}$). By contrast, the Hall conductance of gapped free fermion systems in strictly two-dimensions must be an integer. Similarly, breaking charge conservation realizes a time-reversal-invariant cousin of topological $p + ip$ [38–40] superconductors with Majorana modes in vortex cores. Finally, strong interactions may gap the surface while preserving both symmetries by forming an anomalous topological order [41–45].

II. ENTANGLEMENT SPECTRA OF ANOMALOUS SURFACES

Any surface wave function of a free-fermion SPT may be expressed as

$$|\Phi\rangle_\Lambda = \hat{\Phi}_\Lambda(c^\dagger_{E,i})|0\rangle_\Lambda. \tag{1}$$

Here $\hat{\Phi}_\Lambda$ is an operator-valued function, and $c^\dagger_{E,i}$ creates an electron in a single-particle eigenstate with energy E and additional quantum numbers i. The "empty state" $|0\rangle_\Lambda$ denotes a Fermi sea filled up to the top of the valence band at energy $-\Lambda$. Below energy $-\Lambda$, the surface states merge with the bulk bands, but between $-\Lambda$ and Λ, the surface states are separated from the bulk. A similar surface state can be found in Ref. [46].

The symmetric, noninteracting surface is thus represented by

$$|\Phi\rangle^0_\Lambda = \prod_i \prod_{E=\Lambda}^{\mu} c^\dagger_{E,i}\,|0\rangle_\Lambda, \tag{2}$$

with chemical potential μ, where $|0\rangle_\Lambda$ symbolizes the vacuum state with cutoff Λ [47]. In general, $|\Phi\rangle_\Lambda$ must reduce to $|\Phi\rangle^0_\Lambda$ for $c_{E\to\Lambda}$ to describe a surface state that does not hybridize with the bulk. The cutoff Λ is inevitable due to the anomalous nature of the surface state, but its precise value does not affect local observables.

To test our expectations for the ES of anomalous states, we study the surface of a 3D TI, which hosts a single Dirac cone governed by

$$H_M = \sum_{\boldsymbol{k}} \phi^\dagger_{\boldsymbol{k}}[\boldsymbol{k}\cdot\boldsymbol{\sigma} + M\sigma_z]\phi_{\boldsymbol{k}}. \tag{3}$$

Here, $\phi^\dagger_{\boldsymbol{k}}$ creates electrons with momentum $\boldsymbol{k} = (k_x, k_y)$, $\sigma_x, \sigma_y, \sigma_z$ are Pauli matrices, and M is a time-reversal symmetry-breaking mass. The unnormalized single-particle eigenstates are

$$\boldsymbol{v_k} = \begin{pmatrix} \sqrt{\epsilon + M} \\ \sqrt{\epsilon - M}e^{-i\varphi_{\mathbf{k}}} \end{pmatrix}, \quad \boldsymbol{u_k} = \begin{pmatrix} \sqrt{\epsilon - M}e^{i\varphi_{\mathbf{k}}} \\ -\sqrt{\epsilon + M} \end{pmatrix}, \tag{4}$$

where $\epsilon = \sqrt{k^2 + M^2}$ and $k, \varphi_{\boldsymbol{k}}$ are the magnitude and polar angle of the two-dimensional momentum. The corresponding single-particle energies are $E_{\boldsymbol{v}} = -E_{\boldsymbol{u}} = \epsilon$, and the ground state of H_M is $|\Phi^M\rangle_\Lambda = \prod_{\boldsymbol{k}} \boldsymbol{u_k}\phi^\dagger_{\boldsymbol{k}}\,|0\rangle$. In Appendix A, we show the spectrum of Eq. (3) for spherical geometry. We obtain the ES [6–8] by decomposing the Hilbert space of the surface into two parts, $\mathcal{H} = \mathcal{H}_\alpha \otimes \mathcal{H}_\beta$. The Schmidt decomposition

$$|\Phi\rangle = \sum\nolimits_n e^{-\epsilon'_n/2}|\Phi_{\alpha,n}\rangle \otimes |\Phi_{\beta,n}\rangle, \tag{5}$$

with $|\Phi_{\alpha(\beta),n}\rangle \in \mathcal{H}_{\alpha(\beta)}$ yields the "entanglement energies" ϵ'_n. We numerically compute these numbers for $|\Phi\rangle_\Lambda$ with α, β, the two hemispheres of a sphere with radius R (Fig. 3). For local observables, we would expect universal results when $R^{-1} \ll M \ll \Lambda$. For the ES, we instead find that the number of low-lying λ_i (where $\lambda_i = \frac{e^{-\epsilon'_i}}{1+e^{-\epsilon'_i}}$) grows linearly with

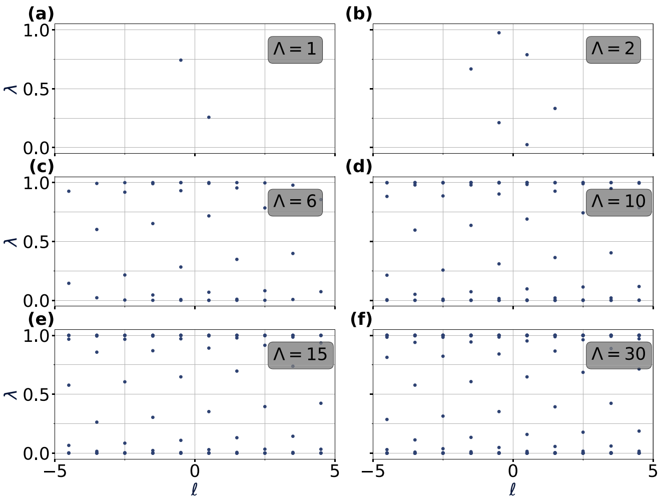

FIG. 2. The entanglement spectra of anomalous surface states are strongly sensitive to the short-distance cutoff. Panels (a)–(f) show the entanglement spectra for 3D topological insulator surfaces with a magnetic mass $M = 2$ and cutoff values $\Lambda = 1, 2, 6, 10, 15, 30$, respectively.

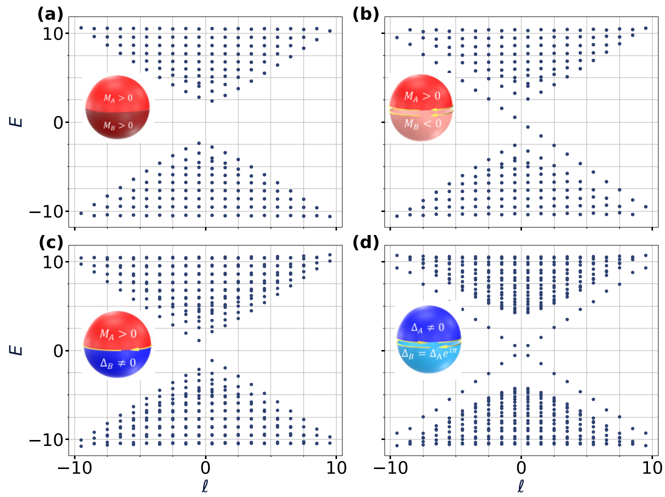

FIG. 4. Physical edge spectra of spherical 3D topological insulator surfaces. In panels (a) and (b), both hemispheres are magnetically gapped. When the masses have equal signs, the spectrum is gapped (a). When they have opposite signs, it hosts a gapless chiral complex fermionic edge mode (b). In panel (c), the lower hemisphere is a proximity-induced s-wave superconductor, hence the spectrum hosts a chiral Majorana mode. In panel (d), both the systems are s-wave superconductors with a phase difference of π. The spectrum hosts two counter-propagating gapless Majorana channels.

the cutoff Λ (cf. Fig. 2). In Fig. 3 panel (c), we show the number of pseudoenergy states as a function of the cutoff for massless and massive Dirac fermions. We attribute this cutoff dependence and the large number of low-lying states to the exposure of the underlying bulk (cf. Fig. 1). As anticipated in the introduction, straightforward computation of the ES of a surface state is not suitable for its identification.

III. RELATIVE ENTANGLEMENT SPECTRA

Our goal is to construct an ES that is cutoff independent and permits the distinction between various surface states. To achieve this, we draw insights from physical surface spectra. Specifically, the interface between two distinct surface phases hosts gapless edge channels whose states are entirely dictated by the neighboring surface phases. Figure 4 shows the energy spectra for a spherical topological insulator with different free-fermion surface states on the upper and lower hemispheres.

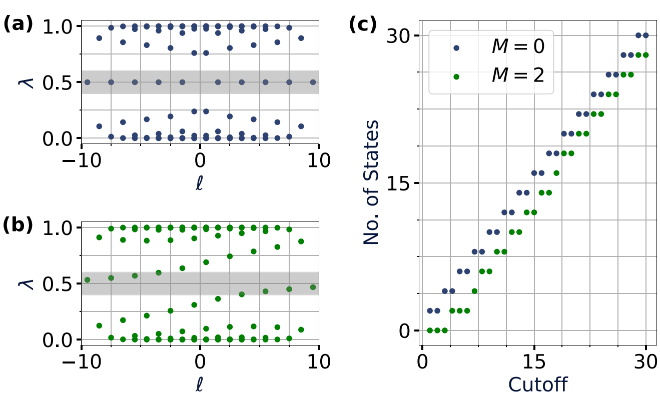

FIG. 3. The entanglement spectra of anomalous surface states exhibit a large number of low-lying states ($\lambda_i \approx 0.5$) that increase with the cutoff. In the x axis, ℓ is the z component of the angular momentum and in the y axis $\lambda = e^{-\epsilon'}/(1 + e^{-\epsilon'})$, where ϵ' is the entanglement energy. λ is also the eigenvalue of the correlation matrix [48]. Panels (a) and (b) show the spectra for a gapless and massive Dirac cone, respectively, with cutoff $\Lambda = 10$. In both cases, the number of states within the shaded low-energy window scales linearly with the cutoff and is thus nonuniversal (c).

Building on this understanding, our strategy is to craft nonanomalous wave functions that encode the boundary between two surface states, labeled A and B. This foundation sets the stage for a more detailed examination of specific surface states. For instance, we begin with a gapped free-fermion surface Hamiltonian

$$H_A = \sum_{\mathbf{k},\sigma=\pm} \sigma \epsilon_A(k) c^{A,\dagger}_{\mathbf{k},\sigma} c^{A}_{\mathbf{k},\sigma}, \tag{6}$$

where $c^A_{\mathbf{k},\pm}$ are the linear combinations of $c_{E,i}$ that diagonalize Eq. (3) with eigenvalues $\pm\epsilon_A$. The ground state wave function of this Hamiltonian is the free-fermion surface state A, represented by

$$|\Phi\rangle^A_\Lambda = \prod_i c^{A,\dagger}_{\mathbf{k},i} |0\rangle_\Lambda. \tag{7}$$

In $|\Phi\rangle^A_\Lambda$, the lower band is completely filled. It can be viewed as a fully gapped vacuum state for the excitations $c^{A,\dagger}_{\mathbf{k},+}$ and $c^A_{\mathbf{k},-}$. We note that linear combinations $\psi^\dagger_A(\boldsymbol{r})$ of the particle excitations $c^{A,\dagger}_{\mathbf{k},+}$ can be localized in real space. By contrast, linear combinations formed by Dirac particles $c_{E,i}$ with $E > 0$ can only be quasilocalized with power-law decay. As such, $\{\psi_A\}$ can be used to create a local puddle of a different surface state B, i.e.,

$$|\Phi\rangle^{\text{Puddle}}_\Lambda = \hat{\Phi}^{\text{Puddle}}_{A,\Lambda}(\psi_A)\, |\Phi\rangle^A_\Lambda\,. \tag{8}$$

The spatial boundary between A and B is fully encoded in $\hat{\Phi}^{\text{Puddle}}_{A,\Lambda}$, which is "conventional," i.e., expressed in terms of local orbitals. Following the logic of entanglement spectra, we expect the same boundary can be inferred by letting the B puddle cover the entire surface and then computing the entanglement spectrum of the resulting $\hat{\Phi}^{\text{Puddle}}_{A,\Lambda}(\psi_A)$.

To implement this reasoning technically, we replace the particle creation operator $c^{A,\dagger}_{\mathbf{k},-}$ with the annihilation operator of a hole $d^{A}_{-\mathbf{k},-}$. The reference state Φ^A_Λ then satisfies

$$c^{A}_{\mathbf{k},+}\,|\Phi\rangle^A_\Lambda = 0,\ \ d^{A}_{\mathbf{k},-}\,|\Phi\rangle^A_\Lambda = 0, \tag{9}$$

and the empty state is $|0\rangle_\Lambda = \prod_i d^{A,\dagger}_{\mathbf{k},-}\,|\Phi\rangle^A_\Lambda$. Next, we introduce a gapped surface state B, which need not be one of free fermions. Its general form is given by Eq. (1), i.e., $|\Phi\rangle^B_\Lambda = \hat{\Phi}_{B,\Lambda}(c_{E,i})\,|0\rangle_\Lambda$. Next, we express $c_{E,i}$ in terms of $c^{A,\dagger}_{\mathbf{k},-}, d^{A}_{-\mathbf{k},-}$ and use the expression for $|0\rangle_\Lambda$ given below Eq. (9) to obtain

$$\begin{aligned}|\Phi\rangle^B_\Lambda &= \hat{\Phi}_{B,\Lambda}\big(\{c_{E,i}\} \to \{d^{A}_{-\mathbf{k},-}, c^{A,\dagger}_{\mathbf{k},+}\}\big)\prod_i d^{A,\dagger}_{-\mathbf{k},-}\,|\Phi\rangle^A_\Lambda\\ &\equiv \hat{\Psi}^A_B\big(d^{A,\dagger}_{-\mathbf{k},-}, c^{A,\dagger}_{\mathbf{k},+}\big)\,|\Phi\rangle^A_\Lambda\,. \end{aligned}\tag{10}$$

Notice that we have used normal ordering to reach from the first to the second line. The second line defines the wave function $\hat{\Psi}^A_B$, which does not depend on the cutoff directly so long as A, B are both surface states by the definition of Sec. II. Since $\hat{\Psi}^A_B$ depends on both A and B, we dub it relative wave function. We can now treat it as any conventional wave function and compute its ES as usual; the result is the relative entanglement spectrum between states A and B. We now proceed by numerically calculating the relative ES of various 3D TI surface states and comparing them with the physical edge spectra. Subsequently, we elaborate on the relative wave functions and provide an analytical perspective on their ES.

IV. NUMERICAL RESULTS

A. Free fermions

We compute the relative ES described above for various surface states of a spherical 3D TI. For $|\Phi^A\rangle_\Lambda$, we take states with a magnetic or superconducting gap, i.e., the ground states of Eq. (3) or of

$$H^{\text{SC}}_{\Delta_s} = H_0 + \Delta_s \sum_k [\phi_{k,\uparrow}\phi_{-k,\downarrow} + \text{H.c.}]. \tag{11}$$

To establish that the relative ES reproduces the boundary between anomalous surfaces and is cutoff independent, we also take the second state to be one of free fermions. In this case, the ES can be efficiently computed using the correlation matrix of particles and holes [13,48–54] (see also Appendix B). The corresponding physical energy spectra are well known. They are summarized, e.g., in Sec. V of the review Ref. [28] and shown for the spherical geometry in Fig. 4.

Figure 5 shows the relative ES for various choices of the gapped free-fermion systems A, B. In Fig. 5(a), we take A and B to be different representatives of the same phase. Their relative ES is gapped, as expected. In (b), we take both A and B as magnetically gapped, but with opposite signs. Here, the ES describes a chiral Dirac fermion, matching a physical boundary between the same phases. Panel (c) depicts the relative ES between a state with a magnetic gap and a state with a superconducting gap. The Majorana mode in the ES matches the physical energy spectrum at such a boundary. Finally, panel (d) shows the case where A and B are superconductors with a phase difference π. Again, the ES correctly reproduces the expected helical Majorana edge states. Additional data about the dependence of the spectra on the magnitude of the masses are shown in Appendix D. In Appendix E, we show the relative ES for a 1D anomalous edge state.

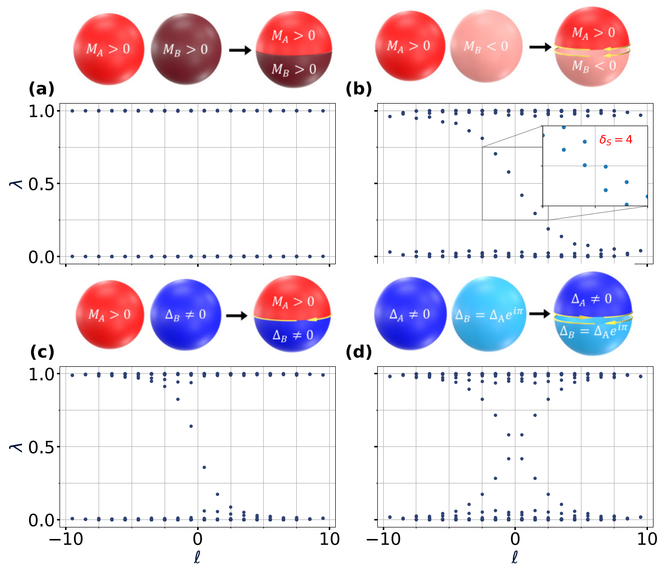

FIG. 5. The relative entanglement spectra of different 3D topological insulator surface states match the energy spectra at a physical boundary between the same states. For magnetically gapped states with the same sign, the entanglement spectrum is gapped, as shown in (a) for $M_A = 4$ and $M_B = 6$. For opposite signs, there is a chiral edge state, shown in (b) for $M_A = 4$ and $M_B = -4$. The edge state corresponds to a complex fermion and is split by breaking charge conservation (inset). Similarly, the relative entanglement spectrum of a magnetically gapped and a paired state exhibits a single chiral Majorana mode, shown in (c) for $M_A = 4$, $\Delta_B = -4$. For two paired states with π phase difference we find a nonchiral state with helical Majorana fermions, see (d) where $\Delta_A = 2$, $\Delta_B = -8$.

B. Interacting states

We verify that the relative ES extends beyond free-fermion states by studying Dirac electrons with contact interactions U, i.e., the model

$$H_{\text{Int}} = H_0 + U\int_{\boldsymbol{r}\in S^2}\phi^\dagger_\downarrow(\boldsymbol{r})\phi_\downarrow(\boldsymbol{r})\phi^\dagger_\uparrow(\boldsymbol{r})\phi_\uparrow(\boldsymbol{r}). \tag{12}$$

This model preserves time-reversal symmetry and the z component of the total angular momentum $L^T_z = \sum_i \ell_i$. Its phase diagram was obtained in Ref. [55] using exact diagonalization, and we also use the same method to obtain the ground state.

For strong repulsive interactions, the system is in a ferromagnetic phase with a twofold degenerate ground state (weakly split in a finite system). We use the even combination with negative magnetization as state B and massive

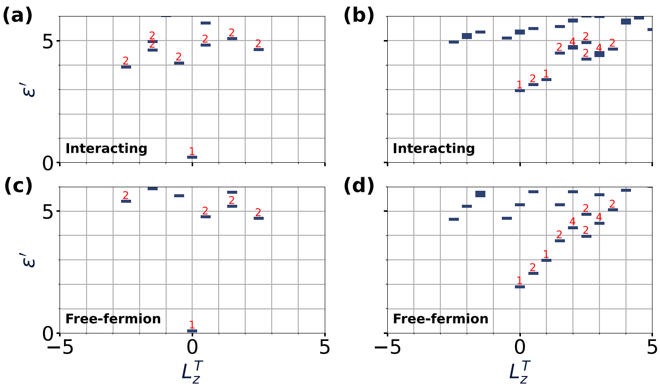

FIG. 6. The relative entanglement spectra between repulsive Dirac electrons and massive noninteracting electrons clearly identify the phase of the former. When the sign of the spontaneous magnetization matches the mass of the free-fermion state, the entanglement spectrum is gapped (a). When they are opposite, there is a single chiral state (b). Panels (c) and (d) show the corresponding many-body entanglement spectra for free-fermion wave functions with the same cutoff. The degeneracies of the pseudoenergies are indicated in red.

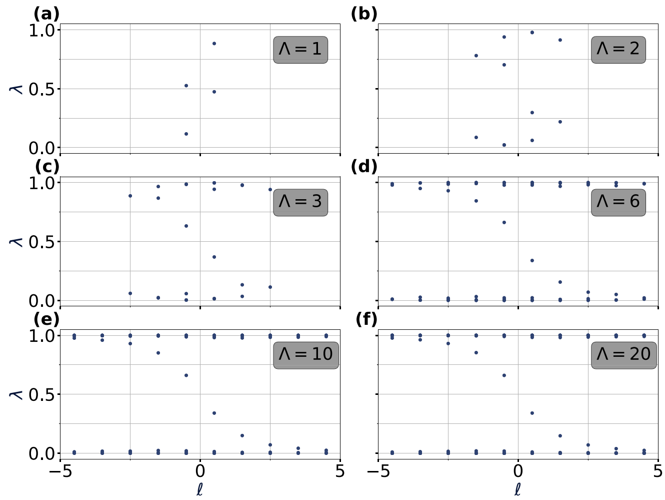

FIG. 7. The relative entanglement spectra of anomalous surface states depend only weakly on the cutoff. Panels (a)–(f) show the spectra for $M_A = 2$, $M_B = -2$, and $\Lambda = 1, 2, 3, 6, 10, 20$, respectively. The low-lying states become insensitive to the cutoff for $\Lambda \gtrsim 3$.

Dirac fermions with $M_A = -2$ or $M_A = 2$ for A. Our results for 12 particles and 24 single-particle states are shown in Fig. 6. Despite the relatively small system size, the ES clearly identifies state B. If its magnetization matches the sign of the mass in A, there is a large gap in the ES [Fig. 6(a)]. For opposite signs, it is gapless and exhibits a left-moving chiral mode [Fig. 6(b)]. These spectra qualitatively agree with the analogous free-fermion spectra [Figs. 6(c) and 6(d)].

C. Cutoff dependence

The cutoff dependence of the ES for a magnetically gapped TI surface is shown in Fig. 2. The number of low-lying entanglement-energy levels ($\lambda \approx 0.5$) increases linearly with the cutoff. As such, the ES is dominated by nonuniversal features. By contrast, the low-lying states in the relative ES quickly converge to their $\Lambda \to \infty$ values, see Fig. 7. There is an appreciable entanglement gap already for a cutoff as small as $\Lambda = 3$.

V. RELATIVE HAMILTONIANS

Having established the utility of relative ES numerically, we return to its analytical interpretation. It is illuminating to construct a parent Hamiltonian whose ground state is the relative wave function. We thus define the relative Hamiltonian as the parent Hamiltonian H^B of a surface phase B expressed in terms of the excitations $c^A_{i,\pm}$. Since A and B are surface states by assumption, the relative Hamiltonian is bounded from below [56].

As a concrete example, we consider massive Dirac fermions, described by Eq. (3) for A. Using Eq. (4), we write

$$H_{M_A} = \sum\nolimits_{\boldsymbol{k}} \epsilon_A c^{A,\dagger}_{\boldsymbol{k},\pm} c^A_{\boldsymbol{k},\pm}, \quad c^A_{\boldsymbol{k},\pm} = \frac{1}{2\sqrt{\epsilon_A}}[v^*_{\boldsymbol{k}}\phi_{\boldsymbol{k}} \pm u^*_{\boldsymbol{k}}\phi^\dagger_{-\boldsymbol{k}}], \tag{13}$$

and the ground state satisfies $c^A_{\boldsymbol{k},\pm}|\Phi_{M_A}\rangle = 0$. For B, we take Dirac fermions with a mass M_B, also described by Eq. (3). Expressing their Hamiltonian in terms of $c^A_{\boldsymbol{k},\pm}$, we find $H_{M_B} = H^+ + H^-$ with

$$H^\pm = \sum_{\boldsymbol{k}} E^\pm_k c^{A,\dagger}_{\boldsymbol{k},\pm} c^A_{\boldsymbol{k},\pm} + \sum\nolimits_{\boldsymbol{k}} \left[\Delta^\pm_{\boldsymbol{k}} c^A_{\boldsymbol{k},\pm} c^A_{-\boldsymbol{k},\pm} + \mathrm{H.c}\right], \tag{14}$$

where

$$\begin{aligned} E^\pm_k &= \epsilon_A + M_A(M_B - M_A)/\epsilon_A, \\ \Delta^\pm_{\boldsymbol{k}} &= \pm(M_A - M_B)ke^{i\varphi_{\boldsymbol{k}}}/\epsilon_A. \end{aligned} \tag{15}$$

For either choice of sign, Eq. (14) describes a superconductor of spinless fermions with chiral p-wave pairing. The U(1) symmetry of the surface states A and B is reflected in $E^+ = E^-$ and $|\Delta^+| = |\Delta^-|$. For an equal sign of the masses M_A and M_B, the functions $E^\pm_k$ are positive for all k. The chemical potential of $c^A_{\boldsymbol{k},\pm}$ thus lies beyond the bottom of the band and $H_\pm$ each describes a topologically trivial strongly paired superconductor. For opposite signs, the chemical potential lies within the band, and the superconductors are topological. A boundary where the mass changes sign hosts two chiral Majorana fermions or, equivalently, one chiral complex fermion.

A more detailed derivation for this relative Hamiltonian is given in Appendix C.

As a second example, we take A as before and choose B as a superconducting surface state described by Eq. (11). We find

$$\begin{aligned} H^{\mathrm{SC}}_{\Delta_s} &= H^+ + H^-, \\ E^\pm_k &= k^2/\epsilon_A \pm \Delta_s, \\ \Delta^\pm &= ke^{\pm i\varphi_{\boldsymbol{k}}}\Delta_s. \end{aligned} \tag{16}$$

For any nonzero Δ_s, one of the flavors is strongly paired, and the second is weakly paired. Thus, there is always a single chiral Majorana at the interface of H_{Δ_s} with the reference vacuum.

Alternatively, a superconducting surface can also serve as a reference system. To identify its excitations, we diagonalize the model of Eq. (11), i.e., the Hamiltonian

$$H_{\Delta_s}^{\mathrm{SC}} = \sum_{\mathbf{k}} [\phi_{\mathbf{k},\uparrow}^\dagger (k e^{-i\varphi_{\mathbf{k}}} \phi_{\mathbf{k},\downarrow} + \Delta_s \phi_{-\mathbf{k},\downarrow}^\dagger) + \mathrm{H.c.}]. \tag{17}$$

We begin with a Bogoliubov transformation to introduce new fermions $\zeta_{\mathbf{k},\downarrow}$:

$$\zeta_{\mathbf{k},\downarrow} = \frac{1}{\epsilon_\Delta} (k e^{-i\varphi_{\mathbf{k}}} \phi_{\mathbf{k},\downarrow} + \Delta_s \phi_{-\mathbf{k},\downarrow}^\dagger), \tag{18}$$

with $\epsilon_\Delta = \sqrt{k^2 + |\Delta_s|^2}$. They satisfy the usual anticommutation relations:

$$\begin{aligned} &\{\zeta_{\mathbf{k},\downarrow}^\dagger, \zeta_{\mathbf{k}',\downarrow}\} = \delta_{\mathbf{k},\mathbf{k}'}, \\ &\{\zeta_{\mathbf{k},\downarrow}, \zeta_{\mathbf{k}',\downarrow}\} = \{\zeta_{\mathbf{k},\downarrow}^\dagger, \zeta_{\mathbf{k}',\downarrow}^\dagger\} = 0, \\ &\{\phi_{\mathbf{k},\uparrow}^\dagger, \zeta_{\mathbf{k}',\downarrow}\} = \{\phi_{\mathbf{k},\uparrow}^\dagger, \zeta_{\mathbf{k}',\downarrow}^\dagger\} = 0. \end{aligned} \tag{19}$$

Substituting Eq. (18) into Eq. (17) yields

$$H_{\Delta_s}^{\mathrm{SC}} = \sum_{\mathbf{k}} \epsilon_\Delta (\phi_{\mathbf{k},\uparrow}^\dagger \zeta_{\mathbf{k},\downarrow} + \zeta_{\mathbf{k},\downarrow}^\dagger \phi_{\mathbf{k},\uparrow}). \tag{20}$$

Introducing another set of fermion operators as

$$\chi_{\mathbf{k},+} = \frac{1}{\sqrt{2}} (\phi_{\mathbf{k},\uparrow} + \zeta_{\mathbf{k},\downarrow}), \quad \chi_{\mathbf{k},-} = \frac{1}{\sqrt{2}} (\phi_{-\mathbf{k},\uparrow}^\dagger - \zeta_{-\mathbf{k},\downarrow}^\dagger), \tag{21}$$

we finally obtain

$$H_{\Delta_s}^{\mathrm{SC}} = \sum_{\mathbf{k}} \epsilon_\Delta (\chi_{\mathbf{k},+}^\dagger \chi_{\mathbf{k},+} + \chi_{\mathbf{k},-}^\dagger \chi_{\mathbf{k},-}). \tag{22}$$

Consider now a surface state with different pairing Δ_s'. In terms of the operators defined by Eq. (21), its Hamiltonian is

$$H_{\Delta_s'}^{\mathrm{SC}} = H^\pm + \sum_{\mathbf{k}} \left(\Delta_{\mathbf{k}}^M \chi_{\mathbf{k},+}^\dagger \chi_{-\mathbf{k},-}^\dagger + \mathrm{H.c.}\right), \tag{23}$$

where $H^\pm$ is given by Eq. (14) with dispersion

$$E_k^\pm = \left(k^2 + \frac{\Delta_s' \Delta_s^* + \Delta_s'^* \Delta_s}{2}\right) \Big/ \epsilon_\Delta, \tag{24}$$

and mean-field pairing

$$\Delta_{\boldsymbol{k}}^- = k e^{i\varphi_{\mathbf{k}}} (\Delta_s - \Delta_s')/2\epsilon_\Delta, \tag{25}$$

where $\Delta_{\boldsymbol{k}}^+ = (\Delta_{\boldsymbol{k}}^-)^*$. The final term

$$\Delta_{\boldsymbol{k}}^M = (\Delta_s'^* \Delta_s - \Delta_s' \Delta_s^*)/\epsilon_\Delta \tag{26}$$

vanishes when the phases of Δ_s' and Δ_s differ by π. In that case, H^+ and H^- decouple. Each describes a superconductor with $k_x \pm i k_y$ pairing and negative "chemical potential" $(\Delta_s' \Delta_s^* + \Delta_s'^* \Delta_s)/2$. The boundary of this system hosts a pair of counter-propagating Majorana modes. For other phase differences, the two Majorana modes gap out.

Table I summarizes the possible relative Hamiltonians for various choices of A, B. We note that a simple analytical expression for the ES of H^+ on an infinite cylinder was obtained in Ref. [11] for a particular choice of the functions E_k^+, $\Delta_{\boldsymbol{k}}^\pm$ [57]. For generic parameters and different geometries, a similar expression is unavailable. Still, for free-fermion states, the ES can be efficiently obtained from correlation matrices.

TABLE I. The relative Hamiltonians realize topological $p \pm ip$ superconductors or topologically trivial strongly paired (SP) superconductors depending on the type and sign of the mass terms. The helical edge state arising for opposite superconducting mass terms is protected by time-reversal symmetry.

	Magnetic gap $M^A > 0$	Pairing gap $\Delta^A > 0$
$M^B > 0$	SP and SP	$p - ip$ and SP
$M^B < 0$	$p + ip$ and $p + ip$	$p + ip$ and SP
$\Delta^B < 0$	$p + ip$ and SP	$p + ip$ and $p - ip$
$\Delta^B > 0$	$p - ip$ and SP	SP and SP

VI. DISCUSSION AND CONCLUSIONS

We have generalized entanglement spectroscopy as a tool for identifying phases of matter to SPT surface states. Mapping the boundary between two surface states onto the analogous edge of a nonanomalous state allowed us to invoke the standard ES-edge correspondence. We have demonstrated the utility of relative ES via large-scale numerical simulations of free-fermion and interacting systems.

The most immediate applications of our analysis arise in numerical studies of SPT surfaces, where it may identify nontrivial phases. For example, symmetry preserving surface topological orders are known to be possible on 3D TI and 3D topological superconductor surfaces [41–45,58–61]. Relative ES and the corresponding relative entanglement entropy would be the natural tools for their numerical identification in candidate systems.

Anomalies also arise in systems other than SPT surfaces. For example, in fractional quantum Hall systems at half-filling, an anomalous particle-hole symmetry plays an analogous role to time reversal on the 3D TI surface [62]. Specifically, the orbital ES is mirrored under a particle-hole transformation. As such, it must be nonchiral for a particle-hole symmetric state and cannot represent its edge with a trivial vacuum. We expect that a variant of the relative ES may be advantageous in the context of such states.

Additionally, the methods developed here can prove beneficial for analyzing various one-dimensional spin systems. It is often convenient to fermionize these models via a Jordan-Wigner transformation. The nonlocality of this mapping results in an anomalous theory of fermions [63], suggesting that relative ES will be the appropriate tool.

Finally, relative ES may also be valuable for non anomalous systems. We note that for a band insulator, the relative ES between states with n-1 and n filled band encodes exactly the contribution of the nth band. More generally, relative ES may help identify interacting states with complex edge structures that are not readily deduced from their (many-body) ES. In fact, a variant of this is already known in quantum Hall systems. There, performing a particle-hole transformation prior to a real-space cut [64–66] amounts to computing the relative ES with a $\nu = 1$ quantum Hall state. As a consequence, the ES of "hole conjugate states," such as the anti-Pfaffian, greatly simplify. More generally, obtaining the boundary of an unknown state with multiple two-dimensional phases may help disentangle the contributions from multiple edge modes.

ACKNOWLEDGMENTS

We are indebted to Misha Yutushui for sharing his code for exact diagonalization on the 3D TI surface, and to Jason Alicea and Lesik Motrunich for illuminating discussions on this topic. This work was partially supported by the Deutsche Forschungsgemeinschaft (DFG) under CRC 183 (Project No. 277101999) and the Israel Science Foundation (2572/21).

APPENDIX A: SURFACE STATES OF SPHERICAL TOPOLOGICAL INSULATORS

The single-particle eigenstates on a spherical TI surface [55,67] are given by

$$\phi_{n,\ell,\lambda} = \frac{1}{\sqrt{2}}\begin{pmatrix} Y_{1/2,n+1/2,\ell} \\ \lambda Y_{-1/2,n+1/2,\ell}\end{pmatrix}, \tag{A1}$$

where Y are the monopole harmonics [68,69]. The corresponding energies are $\epsilon_{n,\ell,\lambda} = \lambda n$, where $\lambda = \pm 1$ and n is a positive integer. The angular momentum ℓ takes half-odd integer values in the interval $[-n + 1/2, n - 1/2]$. For any numerical calculation, we implement a cutoff by retaining only $n \leqslant \Lambda$. The spectrum for $\Lambda = 3$ is shown in Fig. 8.

APPENDIX B: ENTANGLEMENT SPECTRA OF CONTINUUM SYSTEMS FROM THEIR CORRELATION MATRIX

The ES of a free fermion system is fully encoded in the correlation matrix [13,48–54]. The latter can be efficiently obtained by inverting the single-particle Hamiltonian H. In continuum models, such as the one describing the 3D TI surface, there is a minor subtlety that is absent on lattice systems. To illustrate this issue, let $\psi_i(\boldsymbol{x})$ with $i = 1, \ldots, N$ be an orthonormal basis of single particle states for the full system. The projections of ψ_i onto any subsystem are generically not orthonormal. Still, standard methods readily obtain orthonormal functions ψ_i^A in A and ψ_i^B in B for the projected ψ_i. As a result, we obtain the decomposition

$$\psi_i(\boldsymbol{r}) = \sum_j \left[\alpha_{ij}\psi_j^A(\boldsymbol{r}) + \beta_{ij}\psi_j^B(\boldsymbol{r})\right]. \tag{B1}$$

Notice that the N states of the original system are encoded in $2N$ states after this decomposition. Consequently, Eq. (B1) is not invertible, and the correlation matrix for states within A, cannot be directly obtained from the full Hamiltonian. Equivalently, inserting Eq. (B1) into any Hamiltonian enlarges the Hilbert space by N single-particle states with zero eigenvalue.

To circumvent this problem, we enlarge the original Hilbert space by N single-particle states at infinite energy. Specifically, let $v_i = (\alpha_{i,1}^0 \ldots \alpha_{i,N}^0\ \beta_{i,1}^0 \ldots \beta_{i,N}^0)$ be the null vectors of the matrix

$$\mathcal{M} = \begin{pmatrix} \alpha_{11} & \ldots & \alpha_{1N} & \beta_{11} & \ldots & \beta_{1N} \\ \vdots & \vdots & \vdots & \vdots & \vdots & \vdots \\ \alpha_{N1} & \ldots & \alpha_{NN} & \beta_{N1} & \ldots & \beta_{NN}\end{pmatrix}. \tag{B2}$$

Then the wave functions

$$\psi_i^0(\boldsymbol{r}) \equiv \sum_j \left[\alpha_{ij}^0\psi_j^A(\boldsymbol{r}) + \beta_{ij}^0\psi_j^B(\boldsymbol{r})\right] \tag{B3}$$

supplement Eq. (B1) to yield an invertible transformation between ψ_i, ψ_i^0 and a_i, b_i. Finally, we modify the single particle Hamiltonian according to $H \to H + H'$ with $\langle\psi_i|H'|\psi_j\rangle = \langle\psi_i^0|H'|\psi_j\rangle = 0$, and $\langle\psi_i^0|H'|\psi_j^0\rangle = m\delta_{ij}$ with $m \to \infty$ to ensure that the additional states do not affect the spectrum or the correlations. After these modifications, the correlation matrix and ES can be computed as in lattice systems.

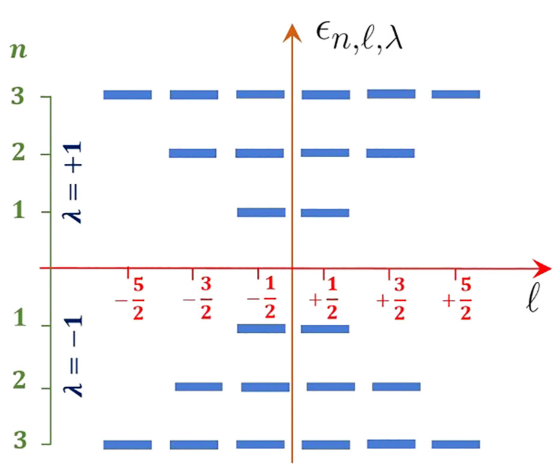

FIG. 8. Spectrum of a spherical 3D topological insulator surface. States are labeled by the positive integer n, the angular momentum $\ell \in [-n + 1/2, n - 1/2]$, and the particle-hole index $\lambda = \pm$. A cutoff in the n quantum number preserves angular momentum.

APPENDIX C: DETAILED DERIVATION OF RELATIVE HAMILTONIAN

We start with two gapped surface states A and B which correspond to the following two Hamiltonians:

$$H_A = \sum_{\mathbf{k}} |\mathbf{k}|c_{\mathbf{k},+}^\dagger c_{\mathbf{k},+} - |\mathbf{k}|c_{\mathbf{k},-}^\dagger c_{\mathbf{k},-} + m_A c_{\mathbf{k},-}^\dagger c_{\mathbf{k},+},$$

$$H_B = \sum_{\mathbf{k}} |\mathbf{k}|c_{\mathbf{k},+}^\dagger c_{\mathbf{k},+} - |\mathbf{k}|c_{\mathbf{k},-}^\dagger c_{\mathbf{k},-} + m_B c_{\mathbf{k},-}^\dagger c_{\mathbf{k},+}, \tag{C1}$$

where $c_{\mathbf{k},\pm}^\dagger$ creates particles in the upper (or lower) band of the Dirac system with momentum $\mathbf{k} = k(\cos\varphi, \sin\varphi)$. The eigenvalues of the Hamiltonian of system A (reference system) are $\pm\epsilon_A = \pm\sqrt{k^2 + m_A^2}$ and the diagonal operators are given by

$$d_{\mathbf{k},-}^\dagger = \frac{1}{\sqrt{2\epsilon_A}}\left(\sqrt{\epsilon_A - m_A}e^{i\varphi_{\mathbf{k}}}c_{\mathbf{k},+}^\dagger - \sqrt{\epsilon_A + m_A}c_{\mathbf{k},-}^\dagger\right),$$

$$d_{\mathbf{k},+}^\dagger = \frac{1}{\sqrt{2\epsilon_A}}\left(\sqrt{\epsilon_A + m_A}c_{\mathbf{k},+}^\dagger + \sqrt{\epsilon_A - m_A}e^{-i\varphi_{\mathbf{k}}}c_{\mathbf{k},-}^\dagger\right). \tag{C2}$$

The reference Hamiltonian in the diagonal basis is $H_A = \sum_{\mathbf{k}}\sqrt{k^2 + m_A^2}d_{\mathbf{k},+}^\dagger d_{\mathbf{k},+} - \sqrt{k^2 + m_A^2}d_{\mathbf{k},-}^\dagger d_{\mathbf{k},-}$ and the ground state wave function is given by $|\Psi\rangle_A^G = \prod_{\mathbf{k}} d_{\mathbf{k},-}^\dagger|0\rangle$. Our goal is to shift the vacuum to the ground state of the reference Hamiltonian. We replace the creation operator $d_{\mathbf{k},-}^\dagger$ of an electron in the filled Fermi sea with the annihilation operator $f_{-\mathbf{k},-}$ of a hole. Previously, the creation operators were creating electrons, now the operators $d_{\mathbf{k},+}^\dagger$ ($f_{\mathbf{k},-}^\dagger$) create particle (hole) excitation on top of the reference ground state $|\Psi\rangle_A^G$. After the transformation, the reference Hamiltonian becomes

$$H^R = \sum_{\mathbf{k}} \sqrt{k^2+m^2} d^\dagger_{\mathbf{k},+} d_{\mathbf{k},+} + \sqrt{k^2+m^2} f^\dagger_{\mathbf{k},-} f_{\mathbf{k},-}, \quad \text{(C3)}$$

and the ground state is annihilated by both the operators d and f, i.e.,

$$d_{\mathbf{k},+}|\Psi\rangle_A^G = 0, \quad f_{\mathbf{k},-}|\psi\rangle_A^G = 0. \quad \text{(C4)}$$

The original creation operators $c^\dagger_{\mathbf{k},+}$ and $c^\dagger_{\mathbf{k},-}$ in terms of $d^\dagger_{\mathbf{k},+}$ and $f_{-\mathbf{k},-}$ are given by

$$\begin{aligned} c^\dagger_{\mathbf{k},+} &= \frac{1}{\sqrt{2\epsilon_A}}\left(\sqrt{\epsilon_A - m}\, d^\dagger_{\mathbf{k},+} - \sqrt{\epsilon_A + m}\, e^{-i\varphi_{\mathbf{k}}} f_{-\mathbf{k},-}\right), \\ c^\dagger_{\mathbf{k},-} &= \frac{1}{\sqrt{2\epsilon_A}}\left(\sqrt{\epsilon_A + m}\, e^{i\varphi_{\mathbf{k}}} d^\dagger_{\mathbf{k},+} + \sqrt{\epsilon_A - m}\, f_{-\mathbf{k},-}\right). \quad \text{(C5)} \end{aligned}$$

Inserting Eq. (C5) in H_B yields

$$\begin{aligned} H_B &= \sum_{\mathbf{k}} k e^{-i\varphi_{\mathbf{k}}} c^\dagger_{\mathbf{k},+} c_{\mathbf{k},-} + k e^{i\varphi_{\mathbf{k}}} c^\dagger_{\mathbf{k},-} c_{\mathbf{k},+} \\ &\quad + M_B c^\dagger_{\mathbf{k},+} c_{\mathbf{k},+} - M_B c^\dagger_{\mathbf{k},-} c_{\mathbf{k},-} \\ &= \sum_{\mathbf{k}} \frac{k^2 + M_A M_B}{\epsilon_A} d^\dagger_{\mathbf{k},+} d_{\mathbf{k},+} + \frac{k^2 + M_A M_B}{\epsilon_A} f^\dagger_{-\mathbf{k},-} f_{-\mathbf{k},-} \\ &\quad + \frac{(M_B - M_A) k e^{i\varphi_{\mathbf{k}}}}{\epsilon_A} d^\dagger_{\mathbf{k},+} f^\dagger_{-\mathbf{k},-} + \text{H.c.} \quad \text{(C6)} \end{aligned}$$

This is a Hamiltonian with pairing terms. The pairing term of the Hamiltonian couples the operators $d_{\mathbf{k},+}$ and $f_{-\mathbf{k},-}$, but we decouple them by taking even and odd combinations of these operators,

$$\begin{aligned} p_{\mathbf{k},+} &= \frac{1}{\sqrt{2}}(d_{\mathbf{k},+} + f_{\mathbf{k},-}), \\ p_{\mathbf{k},-} &= \frac{1}{\sqrt{2}}(d_{\mathbf{k},+} - f_{\mathbf{k},-}). \quad \text{(C7)} \end{aligned}$$

Replacing (C7) in (C6), we obtain

$$H = H^+ + H^-, \quad \text{(C8)}$$

where

$$H^\pm = \sum_{\mathbf{k}} E^\pm_{\mathbf{k}} p^\dagger_{\mathbf{k},\pm} p_{\mathbf{k},\pm} + \Delta^\pm_{\mathbf{k}} p^\dagger_{\mathbf{k},\pm} p^\dagger_{-\mathbf{k},\pm} + \text{H.c.}, \quad \text{(C9a)}$$

$$E^\pm_{\mathbf{k}} = \frac{k^2 + M_A M_B}{\epsilon_A}, \quad \Delta^\pm_{\mathbf{k}} = \pm\frac{(M_B - M_A) k e^{i\varphi_{\mathbf{k}}}}{\epsilon_A}. \quad \text{(C9b)}$$

Each of $H^\pm$ describes a chiral p-wave SC of spinless fermions.

APPENDIX D: EVOLUTION OF RELATIVE ENTANGLEMENT SPECTRA WITH MAGNETIC MASS

We show the relative ES for $M_A = 3$ as a function of M_B in Fig. 9. For equal signs of M_A and M_B, the gap in the relative ES begins to close as $M_B \to 0$. For opposite signs, the edge state emerges and becomes better resolved with increasing M_B.

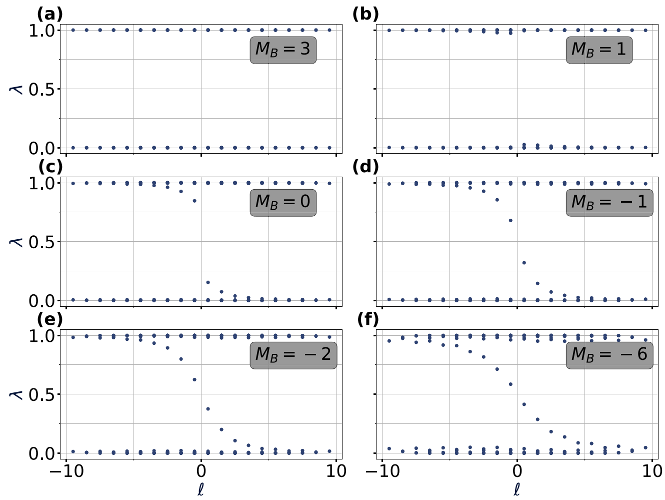

FIG. 9. Evolution of relative entanglement spectra between $M_A = 3$ and different choices of M_B. For opposite signs of the masses, a gapless edge crosses the entanglement gap.

APPENDIX E: RELATIVE ENTANGLEMENT SPECTRA FOR QUANTUM SPIN HALL BOUNDARY STATES

The relative ES applies to any system that permits a gapped free-fermion reference state. As an additional example, we provide results for the two-dimensional quantum spin Hall (QSH) phase on a circular disk. Its physical boundary hosts a single one-dimensional Dirac fermion. In Fig. 10, we show the zero-dimensional relative ES when this boundary becomes gapped by magnetic masses M_A, M_B. The relative ES is gapped for equal signs of the two masses and exhibits a state at zero entanglement energy ($\lambda = 0.5$) for opposite signs. Adding a small pairing term splits this zero mode, see Fig. 10(c). These properties correctly reproduce the known behavior of QSH edge states, where the interface between opposite masses hosts a complex fermion zero mode.

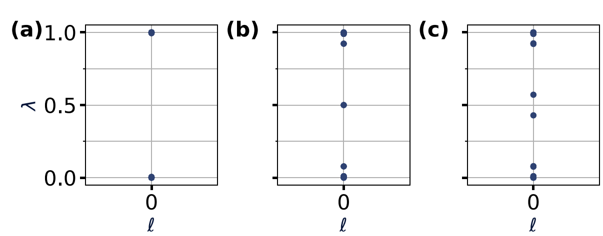

FIG. 10. A 2D quantum spin Hall system on a disk hosts a gapless Dirac fermion on its boundary, i.e., a one-dimensional ring. Breaking time-reversal symmetry opens a gap, as for the 3D topological insulator. The relative entanglement spectrum for a massive edge with the equal sign is gapped, as shown in (a) for $M_A = 2$ and $M_B = 4$. By contrast, there is a zero mode (state with $\lambda = 0.5$) for opposite masses, as shown in panel (b) for $M_A = 2$ and $M_B = -4$. This zero mode splits when a small pairing term is added to the probing system of panel (c).

[1] A. Kitaev and J. Preskill, Topological entanglement entropy, Phys. Rev. Lett. **96**, 110404 (2006).

[2] M. Levin and X.-G. Wen, Detecting topological order in a ground state wave function, Phys. Rev. Lett. **96**, 110405 (2006).

[3] M. Goldstein and E. Sela, Symmetry-resolved entanglement in many-body systems, Phys. Rev. Lett. **120**, 200602 (2018).

[4] J. C. Xavier, F. C. Alcaraz, and G. Sierra, Equipartition of the entanglement entropy, Phys. Rev. B **98**, 041106(R) (2018).

[5] R. Bonsignori, P. Ruggiero, and P. Calabrese, Symmetry resolved entanglement in free fermionic systems, J. Phys. A: Math. Theor. **52**, 475302 (2019).

[6] H. Li and F. D. M. Haldane, Entanglement spectrum as a generalization of entanglement entropy: Identification of topological order in non-Abelian fractional quantum Hall effect states, Phys. Rev. Lett. **101**, 010504 (2008).

[7] X.-L. Qi, H. Katsura, and A. W. W. Ludwig, General relationship between the entanglement spectrum and the edge state spectrum of topological quantum states, Phys. Rev. Lett. **108**, 196402 (2012).

[8] A. Chandran, M. Hermanns, N. Regnault, and B.A. Bernevig, Bulk-edge correspondence in entanglement spectra, Phys. Rev. B **84**, 205136 (2011).

[9] A. M. Turner, Y. Zhang, and A. Vishwanath, Entanglement and inversion symmetry in topological insulators, Phys. Rev. B **82**, 241102(R) (2010).

[10] L. Fidkowski, Entanglement spectrum of topological insulators and superconductors, Phys. Rev. Lett. **104**, 130502 (2010).

[11] J. Dubail and N. Read, Entanglement spectra of complex paired superfluids, Phys. Rev. Lett. **107**, 157001 (2011).

[12] N. Bray-Ali, L. Ding, and S. Haas, Topological order in paired states of fermions in two dimensions with breaking of parity and time-reversal symmetries, Phys. Rev. B **80**, 180504(R) (2009).

[13] E. H. Kim, Characterizing topological order in superconductors via entanglement, J. Phys.: Condens. Matter **26**, 205602 (2014).

[14] N. Regnault, B. A. Bernevig, and F. D. M. Haldane, Topological entanglement and clustering of Jain hierarchy states, Phys. Rev. Lett. **103**, 016801 (2009).

[15] A. M. Läuchli, E. J. Bergholtz, J. Suorsa, and M. Haque, Disentangling entanglement spectra of fractional quantum Hall states on torus geometries, Phys. Rev. Lett. **104**, 156404 (2010).

[16] R. Thomale, A. Sterdyniak, N. Regnault, and B. A. Bernevig, Entanglement gap and a new principle of adiabatic continuity, Phys. Rev. Lett. **104**, 180502 (2010).

[17] R. Thomale, D. P. Arovas, and B. A. Bernevig, Nonlocal order in gapless systems: Entanglement spectrum in spin chains, Phys. Rev. Lett. **105**, 116805 (2010).

[18] H. Yao and X.-L. Qi, Entanglement entropy and entanglement spectrum of the Kitaev model, Phys. Rev. Lett. **105**, 080501 (2010).

[19] L. Fu, C. L. Kane, and E. J. Mele, Topological insulators in three dimensions, Phys. Rev. Lett. **98**, 106803 (2007).

[20] J. E. Moore, Theory of three-dimensional topological insulators, in *Topological Insulators*, Contemporary Concepts of Condensed Matter Science, edited by M. Franz and L. Molenkamp (Elsevier, 2013), Chap. 2, Vol. 6, pp. 35–57.

[21] E. Khalaf, H. C. Po, A. Vishwanath, and H. Watanabe, Symmetry indicators and anomalous surface states of topological crystalline insulators, Phys. Rev. X **8**, 031070 (2018).

[22] A. Kitaev, Periodic table for topological insulators and superconductors, AIP Conf. Proc. **1134**, 22 (2009).

[23] S. Ryu, A. P. Schnyder, A. Furusaki, and A. W. W. Ludwig, Topological insulators and superconductors: tenfold way and dimensional hierarchy, New J. Phys. **12**, 065010 (2010).

[24] A. P. Schnyder, S. Ryu, A. Furusaki, and A. W. W. Ludwig, Classification of topological insulators and superconductors in three spatial dimensions, Phys. Rev. B **78**, 195125 (2008).

[25] Y. Xia, D. Qian, D. Hsieh, L. Wray, A. Pal, H. Lin, A. Bansil, D. Grauer, Y. S. Hor, R. J. Cava, and M. Z. Hasan, Observation of a large-gap topological-insulator class with a single Dirac cone on the surface, Nat. Phys. **5**, 398 (2009).

[26] D. Hsieh, D. Qian, L. Wray, Y. Xia, Y. S. Hor, R. J. Cava, and M. Z. Hasan, A topological Dirac insulator in a quantum spin Hall phase, Nature (London) **452**, 970 (2008).

[27] M. Mogi, Y. Okamura, M. Kawamura, R. Yoshimi, K. Yasuda, A. Tsukazaki, K. S. Takahashi, T. Morimoto, N. Nagaosa, M. Kawasaki, Y. Takahashi, and Y. Tokura, Experimental signature of the parity anomaly in a semi-magnetic topological insulator, Nat. Phys. **18**, 390 (2022).

[28] M. Z. Hasan and C. L. Kane, Colloquium: Topological insulators, Rev. Mod. Phys. **82**, 3045 (2010).

[29] M. Z. Hasan and J. E. Moore, Three-dimensional topological insulators, Annu. Rev. Condens. Matter Phys. **2**, 55 (2011).

[30] X.-L. Qi and S.-C. Zhang, Topological insulators and superconductors, Rev. Mod. Phys. **83**, 1057 (2011).

[31] G. W. Semenoff, Condensed-matter simulation of a three-dimensional anomaly, Phys. Rev. Lett. **53**, 2449 (1984).

[32] E. Fradkin, E. Dagotto, and D. Boyanovsky, Physical realization of the parity anomaly in condensed matter physics, Phys. Rev. Lett. **57**, 2967 (1986).

[33] H. B. Nielsen and M. Ninomiya, A no-go theorem for regularizing chiral fermions, Phys. Lett. B **105**, 219 (1981).

[34] H. B. Nielsen and M. Ninomiya, Absence of neutrinos on a lattice: (I). Proof by homotopy theory, Nucl. Phys. B **185**, 20 (1981).

[35] H. B. Nielsen and M. Ninomiya, Absence of neutrinos on a lattice: (II). Intuitive topological proof, Nucl. Phys. B **193**, 173 (1981).

[36] L. Fu and C. L. Kane, Topological insulators with inversion symmetry, Phys. Rev. B **76**, 045302 (2007).

[37] X.-L. Qi, T. L. Hughes, and S.-C. Zhang, Topological field theory of time-reversal invariant insulators, Phys. Rev. B **78**, 195424 (2008).

[38] N. Read and D. Green, Paired states of fermions in two dimensions with breaking of parity and time-reversal symmetries and the fractional quantum Hall effect, Phys. Rev. B **61**, 10267 (2000).

[39] L. Fu and C. L. Kane, Superconducting proximity effect and majorana fermions at the surface of a topological insulator, Phys. Rev. Lett. **100**, 096407 (2008).

[40] B. A. Bernevig, *Topological Insulators and Topological Superconductors* (Princeton University Press, Princeton, 2013).

[41] P. Bonderson, C. Nayak, and X.-L. Qi, A time-reversal invariant topological phase at the surface of a 3D topological insulator, J. Stat. Mech. (2013) P09016.

[42] C. Wang, A. C. Potter, and T. Senthil, Gapped symmetry preserving surface state for the electron topological insulator, Phys. Rev. B **88**, 115137 (2013).

[43] X. Chen, L. Fidkowski, and A. Vishwanath, Symmetry enforced non-Abelian topological order at the surface of a topological insulator, Phys. Rev. B **89**, 165132 (2014).
[44] M. A. Metlitski, C. L. Kane, and M. P. A. Fisher, Symmetry-respecting topologically ordered surface phase of three-dimensional electron topological insulators, Phys. Rev. B **92**, 125111 (2015).
[45] D. F. Mross, A. Essin, and J. Alicea, Composite Dirac liquids: Parent states for symmetric surface topological order, Phys. Rev. X **5**, 011011 (2015).
[46] Y. Baum and A. Stern, Magnetic instability on the surface of topological insulators, Phys. Rev. B **85**, 121105(R) (2012).
[47] Any state below energy $-\Lambda$ and above energy Λ is occupied and any state in-between is unoccupied.
[48] I. Peschel, Calculation of reduced density matrices from correlation functions, J. Phys. A: Math. Gen. **36**, L205 (2003).
[49] I. Peschel and V. Eisler, Reduced density matrices and entanglement entropy in free lattice models, J. Phys. A: Math. Theor. **42**, 504003 (2009).
[50] I. Peschel and M.-C. Chung, Density matrices for a chain of oscillators, J. Phys. A: Math. Gen. **32**, 8419 (1999).
[51] M.-C. Chung and I. Peschel, Density-matrix spectra for two-dimensional quantum systems, Phys. Rev. B **62**, 4191 (2000).
[52] M.-C. Chung and I. Peschel, Density-matrix spectra of solvable fermionic systems, Phys. Rev. B **64**, 064412 (2001).
[53] J. Borchmann, A. Farrell, S. Matsuura, and T. Pereg-Barnea, Entanglement spectrum as a probe for the topology of a spin-orbit-coupled superconductor, Phys. Rev. B **90**, 235150 (2014).
[54] T. P. Oliveira, P. Ribeiro, and P. D. Sacramento, Entanglement entropy and entanglement spectrum of triplet topological superconductors, J. Phys.: Condens. Matter **26**, 425702 (2014).
[55] T. Neupert, S. Rachel, R. Thomale, and M. Greiter, Interacting surface states of three-dimensional topological insulators, Phys. Rev. Lett. **115**, 017001 (2015).
[56] The Hamiltonians $H^{A,B}$ of any two surface states differ only within a finite energy window and the ground state of H^A is the $c^A_{i,\pm}$ vacuum.
[57] M. Ibañez, J. Links, G. Sierra, and S.-Y. Zhao, Exactly solvable pairing model for superconductors with $p_x + ip_y$-wave symmetry, Phys. Rev. B **79**, 180501(R) (2009).
[58] L. Fidkowski, X. Chen, and A. Vishwanath, Non-Abelian topological order on the surface of a 3D topological superconductor from an exactly solved model, Phys. Rev. X **3**, 041016 (2013).
[59] C. Wang and T. Senthil, Interacting fermionic topological insulators/superconductors in three dimensions, Phys. Rev. B **89**, 195124 (2014).
[60] M. A. Metlitski, L. Fidkowski, X. Chen, and A. Vishwanath, Interaction effects on 3D topological superconductors: surface topological order from vortex condensation, the 16 fold way and fermionic Kramers doublets, arXiv:1406.3032.
[61] S. Sahoo, Z. Zhang, and J. C. Y. Teo, Coupled wire model of symmetric Majorana surfaces of topological superconductors, Phys. Rev. B **94**, 165142 (2016).
[62] D. T. Son, Is the composite fermion a Dirac particle? Phys. Rev. X **5**, 031027 (2015).
[63] A. Karch, D. Tong, and C. Turner, A web of 2d dualities: $\mathbf{Z}_2$ gauge fields and Arf invariants, SciPost Phys. **7**, 007 (2019).
[64] A. Sterdyniak, A. Chandran, N. Regnault, B. A. Bernevig, and P. Bonderson, Real-space entanglement spectrum of quantum Hall states, Phys. Rev. B **85**, 125308 (2012).
[65] J. Dubail, N. Read, and E. H. Rezayi, Real-space entanglement spectrum of quantum Hall systems, Phys. Rev. B **85**, 115321 (2012).
[66] I. D. Rodríguez, S. H. Simon, and J. K. Slingerland, Evaluation of ranks of real space and particle entanglement spectra for large systems, Phys. Rev. Lett. **108**, 256806 (2012).
[67] M. Greiter, Landau level quantization on the sphere, Phys. Rev. B **83**, 115129 (2011).
[68] J. K. Jain, Landau levels, *Composite Fermions* (Cambridge University Press, Cambridge, 2007), pp. 26–76.
[69] F. D. M. Haldane, Fractional quantization of the Hall effect: A hierarchy of incompressible quantum fluid states, Phys. Rev. Lett. **51**, 605 (1983).